Control of Separation on the Flap of a Three-Element High-Lift Configuration

B. Günther[*] and Frank Thiele[†]

Berlin University of Technology, D–10623 Berlin, Germany

R. Petz[‡] and W. Nitsche [§]

Berlin University of Technology, D–10587 Berlin, Germany

J. Sahner[¶], T. Weinkauf[‖] and H.-C. Hege[**]

Zuse Institute Berlin, D–14195 Berlin, Germany

This paper describes a joint experimental and numerical investigation of the control of the flow over the flap of a three-element high-lift configuration by means of periodic excitation. At Reynolds numbers between 0.3×10^6 and 1×10^6 the flow is influenced by periodic blowing or periodic blowing/suction through slots near the flap leading edge. The delay of flow separation by periodic vertical excitation could be identified in the experiments as well as numerical simulations based on the Unsteady Reynolds-averaged Navier-Stokes equations (URANS). As a result, the mean aerodynamic lift of this practically relevant wing configuration could be significantly enhanced. By investigating different excitation frequencies and intensities optimum control parameters could be found. The behaviour of the aerodynamic forces with varying flap deflection angle are measured on a finite swept wing. Scientific visualisation of the numerical simulations of an infinite swept wing allows a detailed analysis of the structures in this complex flow field and the effect of flow control on these.

Nomenclature

c, c_k	clean chord length, flap length ($c_k = 0.254c$)
$c_L, c_{L_{max}}$	lift coefficient, maximum lift coefficient
C_μ	momentum coefficient $C_\mu = 2\frac{H}{c}\left(\frac{u_a}{u_\infty}\right)^2$
f, F^+	frequency of periodic excitation, non-dimensional excitation frequency $F^+ = f\ c_k/u_\infty$
H	slot width ($H = 0.00186c_k$)
Re_c	Reynolds number based on chord length
St	Strouhal number based on flap length
u_∞	inflow velocity
u_a, u_{exc}	amplitude velocity of the perturbation in the slot, excitation velocity
$\alpha, \delta_f, \delta_s$	angle of attack of the main airfoil, flap deflection angle, slat deflection angle
Δt	time step size
Φ	sweep angle

[*]Research Associate, Institute of Fluid Mechanics and Engineering Acoustics, Müller–Breslau–Straße 8, bert.guenther@cfd.tu-berlin.de, +49-30-314-23146, AIAA Student Member.

[†]Professor, frank.thiele@cfd.tu-berlin.de, AIAA Member.

[‡]Research Associate, Institute of Aeronautics and Astronautics, Marchstraße 12, ralf.petz@tu-berlin.de, AIAA Student Member.

[§]Professor, wolfgang.nitsche@tu-berlin.de , AIAA Member.

[¶]Research Associate, Department Visualization and Data Analysis, Takustraße 7, sahner@zib.de.

[‖]Research Associate, Department Visualization and Data Analysis, Takustraße 7, weinkauf@zib.de.

[**]Professor, hege@zib.de.

I.   Introduction

The wings of commercial aircrafts must generate a tremendous amount of lift during take-off and landing in order to reduce ground speeds and runway lengths. Instead of incorporating complex, heavy and expensive multi-element high lift devices, single flaps without slats are desirable. Such flaps can however only be applied if flow separation at high flap angles can be avoided. Experimental investigations[1] as well as numerical simulations[2] have shown that flap separation can be significantly delayed by periodic excitation near the flap leading edge in the case of low and high Reynolds numbers[3] and the lift can be enhanced.

In the past a large number of experimental and numerical studies showed the general effectiveness of flow control for single airfoils (e.g.[4–7]). In most of them, leading edge suction is applied either for transition delay[8] or to affect the separation.[9,10] Other studies employ jet flaps for lift increase and manoeuvring.[11] Unfortunately, most of the earlier control techniques considered have shown little effectiveness.

In further investigations oscillatory suction and blowing was found to be much more efficient with respect to lift than steady blowing. The process becomes very efficient if the excitation frequencies correspond to the most unstable frequencies of the free shear layer, generating arrays of spanwise vortices that are convected downstream and continue to mix across the shear layer. Suction and blowing can be applied tangential to the airfoil surface,[12] perpendicular[13,14] or with cyclic vortical oscillation. In order to create an effective and efficient control method previous studies have been primarily focused on the parameters of the excitation apparatus itself. Overviews are given by Wygnanski and Gad-el-Hak.[15,16]
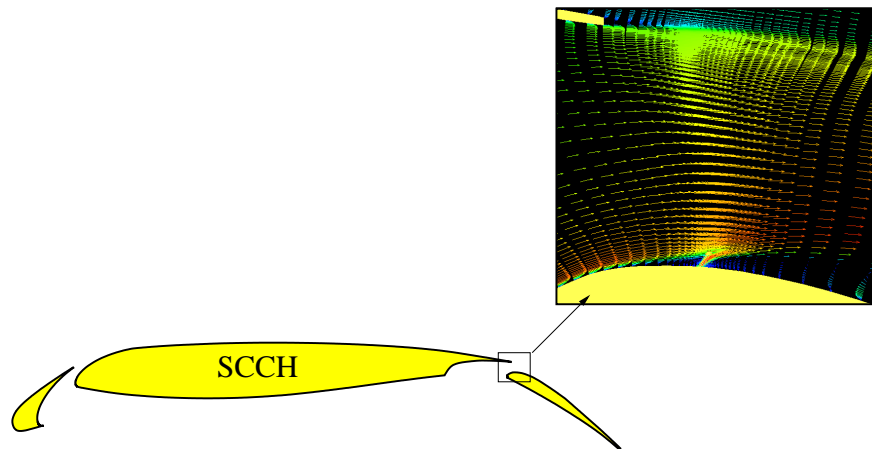

Figure 1. Active flow control by means of vertical suction and blowing at the flap, applied to three-element configuration.

The paper describes a joint numerical and experimental investigation of the control of the flow over the flap of a three-element high-lift configuration by means of periodic excitation.[17] An unsteady wall jet emanating from the single slotted flap shoulder close to the leading edge (figure 1) is used to excite the flow and thus provoke either delay of separation or reattachment.[18] The configuration investigated features a swept wing with extended slat and a single slotted fowler flap. As the flap deflection angle is increased the flow separates from the flap resulting in loss of lift and an increase in drag.

The numerical part mainly focuses on the mechanisms of separation control by analyzing flow field structures at different excitation parameters. The methods of feature-based extraction will be used to identify large scale and dominant structures in the unforced and excited flow field. The experiment is conducted using a half-model with finite span, wing sweep and fuselage whereas the numerical investigation is at this stage carried out on a swept wing of infinite span (without fuselage) in order to study the impact of different excitation parameters more quickly and efficiently. The main emphasis of the experimental investigation lies on the overall lift and drag improvement by measuring integral values. Hence, this joint approach drawing on CFD and experiment will further improve the knowledge of controlling the flow in a three-dimensional flow field.

American Institute of Aeronautics and Astronautics

II.   Numerical Method

The numerical test model represents the practically-relevant *SCCH* (**S**wept **C**onstant **C**hord **H**alf - model) high-lift configuration, which has already been used for several experimental studies targeting passive flow and noise control concepts.[19–21] In the experiments, the three-dimensional wing has a sweep angle of $\Phi = 30°$ and a constant chord length in the spanwise direction. The numerical investigation is mainly focused on a wing with infinite span in order to reduce the computational costs. The simulation of this infinite wing represents only one part of the three-dimensional effects generated by the sweep.
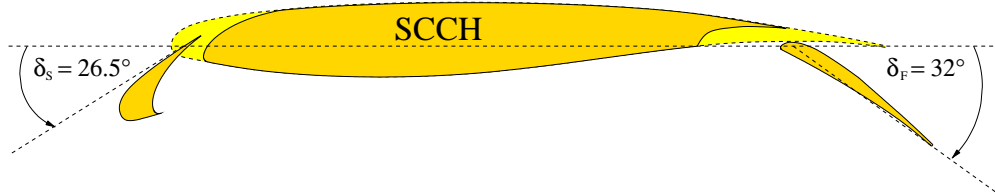

Figure 2.   Sketch of the original SCCH high-lift-configuration.

The typical three-component setup consists of the main airfoil equipped with an extended slat with $0.158\,c$ relative chord length and an extended flap which has a relative chord length of $c_k = 0.254\,c$ (figure 2). All profiles have blunt trailing edges. The flap is situated at a fixed position underneath the trailing edge, forming a gap of $0.0202\,c$ and an overlap of $0.0075\,c$. The flap deflection angle was increased from the base value (32°) in precursor, steady simulations. The detachment position of the flow on the upper flap surface stagnates upstream from a flap deflection angle of 37 degrees. The angle of attack is fixed at 6 degrees for the whole configuration. This angle of attack is situated in the typical range of approach for civil aircraft. In addition, the flow over the flap is detached whereas the flow over the slat and the main wing are still fully attached. With these settings the area of separated flow above the flap is maximised and better suited to the application of active flow control (figure 3).

In all numerical investigations the freestream velocity corresponds to a Reynolds number of $Re_c = 10^6$, based on the chord of the clean configuration (with retracted high-lift devices). This high Reynolds number is chosen to demonstrate the relevance to industrial applications.
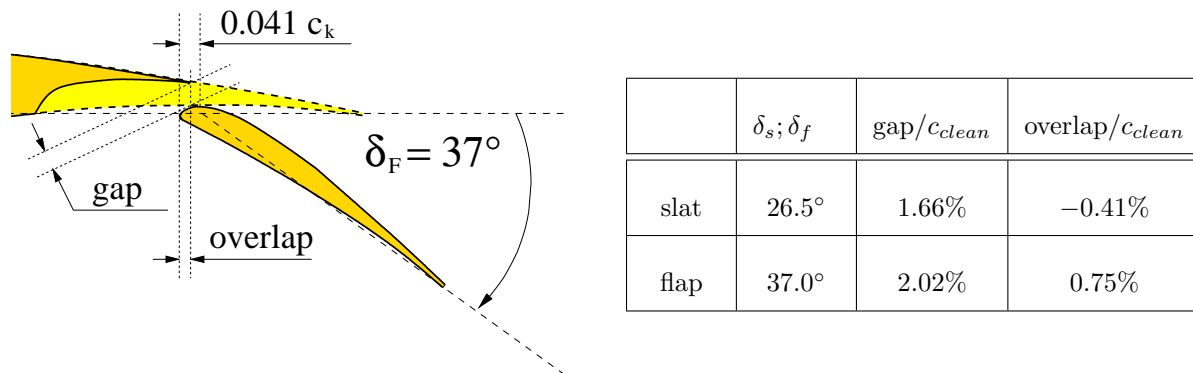

	$\delta_s; \delta_f$	gap/c_{clean}	overlap/c_{clean}
slat	26.5°	1.66%	−0.41%
flap	37.0°	2.02%	0.75%

Figure 3.   Details of the geometry between main airfoil and flap.

All computational investigations are carried out using the numerical code *ELAN* that was developed at the Institute of Fluid Mechanics and Engineering Acoustics of the TU Berlin. The numerical method applied is based on a three-dimensional incompressible Finite-Volume scheme for solution of the Reynolds-averaged Navier-Stokes equations. The three-dimensional method is fully implicit and of second order accuracy in space and time. Based on the SIMPLE pressure correction algorithm, a co-located storage arrangement for all quantities is applied. Convective fluxes are approximated by TVD.

II.A.   Turbulence Modelling

The simulation program can be run in URANS mode, solving the *Unsteady Reynolds-averaged Navier-Stokes equations* using statistical turbulence models as well as in a mode for *Large-Eddy Simulation* (LES) or

American Institute of Aeronautics and Astronautics

combinations of both. In previous URANS investigations with a large variety of different one- and two-equation turbulence models as well as Explicit Algebraic Reynolds-stress Models (EARSM) the LLR k-ω model by Rung[22] exhibited the best overall performance for steady and unsteady airfoil flows with large separation.[23] It represents an improved two-equation eddy-viscosity model formulated with special respect to the realizability conditions.

II.B. Computational Mesh

Figure 4 shows the mesh around the slat, the main airfoil and the flap. All profiles have blunt trailing edges. The dimensions of the computational domain are 15 chords forward, above and below the configuration and 25 chords behind. Figure 4(b) shows the two-dimensional mesh around entire configuration. The computational c-type mesh consists of 90,000 cells in total. The non-dimensional wall-distance of the first cell centre remains below $Y^+ = 1$ over the entire surface.

The three-dimensional mesh is based on an expansion of the two-dimensional mesh into the third direction (4(a)). For consideration of an infinite swept wing 16 layers of the two-dimensional mesh are combined to resolve a three-dimensional wing section using 1,300,000 cells in total. The infinite character is simulated by means of periodic boundary conditions.
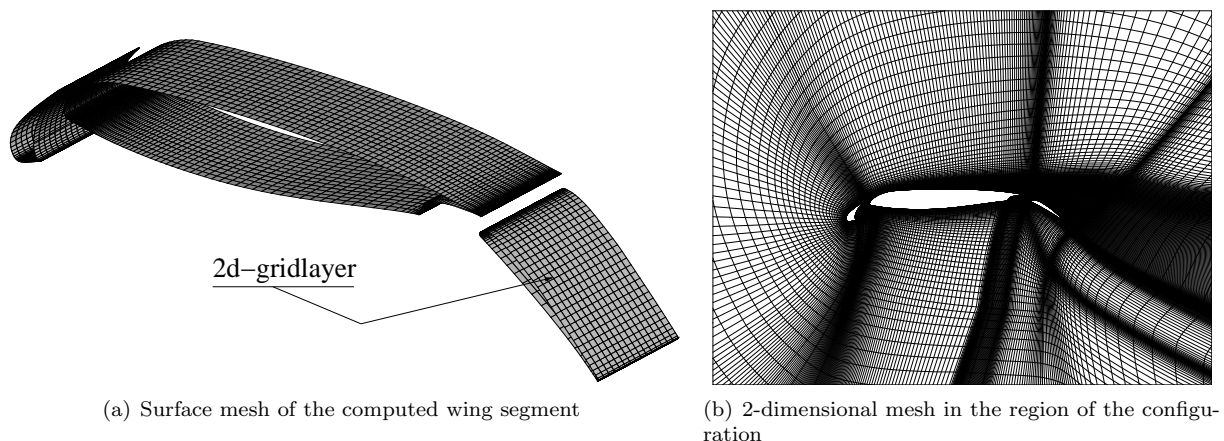

(a) Surface mesh of the computed wing segment

(b) 2-dimensional mesh in the region of the configuration

Figure 4. Computational mesh

II.C. Time Step Size

From initial numerical investigations of the configuration without excitation, characteristics of the unsteady behaviour are already known. A separate study of the influence of time step size indicated that a typical time step of $\Delta t = 4.2 \times 10^{-3} \, c/u_\infty$ is sufficient to obtain results independent of the temporal resolution. All computations presented here are based on $\Delta t = 2.1 \times 10^{-3} \, c/u_\infty$ which allows a resolution of 120 time steps per oscillation cycle for a non-dimensional oscillating frequency of $F^+ = 1$.

II.D. Boundary Conditions

At the wind tunnel entry all flow quantities including the velocity components and turbulent properties are prescribed. The level of turbulence at the inflow is set to $Tu = \frac{1}{u_\infty}(\frac{2}{3}k)^{1/2} = 0.1\%$ and the turbulent viscosity $\mu_t/\mu = 0.1$. At the outflow a convective boundary condition is used that allows unsteady flow structures to be transported outside the domain.

The complete airfoil and flap surface is modeled as a non-slip boundary condition. As the resolution is very fine, a low-Re formulation is applied. The wind tunnel walls are neglected in the far field.

To model the excitation apparatus, a periodic suction/blowing type boundary condition is used. The perturbation to the flow field is introduced through the inlet velocity on a small wall section representing

American Institute of Aeronautics and Astronautics

the excitation slot:

$$u_{exc}(t) = u_a \cdot sin \left[\left(2\pi \frac{u_\infty}{c_k} F^+ \right) \cdot t \right] \qquad \text{with} \qquad u_a = u_\infty \sqrt{\frac{c}{H} C_\mu} \qquad (1)$$

where F^+ is the non-dimensional perturbation frequency, C_μ is the non-dimensional steady momentum blowing coefficient, H is the slot width ($H = 0.00186 c_k$) and u_a is the amplitude velocity of the perturbation oscillation. The oscillating jet is emitted perpendicular to the wall segment of the excitation slot, and is located at 4.1% chord behind the flap leading edge (figure 3).

III. Experimental set-up

In contrast to the numerical investigation which features a swept wing with infinite span, the experiments are conducted using a half model with finite span wing. The high-lift layout (flap and initial flap settings) is identical to the one used in the numerical part (see fig. 2). The wing has a half span of 1120mm and is connected to a generic fuselage section. The investigation is conducted in a closed-circuit wind tunnel with a maximum free speed of $40\,\text{m/s}$ and a test section of $2000\,\text{mm}$ x $1400\,\text{mm}$ (w x h). Figure 5 shows a photo of the model in the test section and a sketch of the basic experimental set-up. In order to measure the
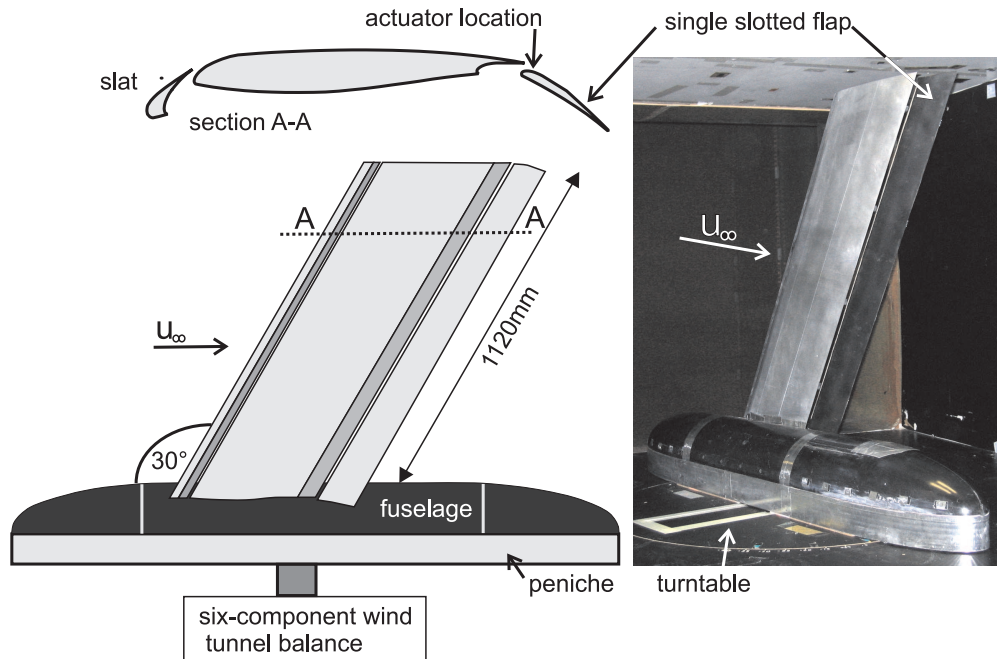

Figure 5. Swept constant chord half model with extendable slat and flap system.

influence of periodic forcing on the aerodynamic forces and moments acting on the model, a six-component balance installed underneath the test section is used. This allows for a simultaneous and instantaneous data acquisition and comparison of unexcited and excited flow cases.

The flap is connected to the main wing by four computer-controlled linear actuators allowing very precise and automated positioning of the flap deflection angle δ_f. However, if the deflection angle of the flap is changed, gap and overlap are altered as well and are not adjusted to the initial landing configuration settings. This differs from the numerical investigations. As the angle of attack α and δ_f are both remote-controlled, fast changes of geometric settings are possible, which is important in an active separation control experiment. Because of the small dimensions of the model with a wing clean chord of only $c = 450\,mm$, installation of a powerful but small flow control actuator into the flap is difficult. Particularly due to the fact that this specific model was never intended to be used as a flow control model the implementation of actuators is not ideal. The main wing section is made of machined aluminium and could not be changed in order to place actuators in the spacious main wing. Hence, a new flap was built using glass-fibre reinforced plastics to allow for actuator placement inside the flap. Nevertheless, the hollow flap still has insufficient room to place most

American Institute of Aeronautics and Astronautics

of the existing flow control actuators inside the flap that produce a zero net mass flux jet, e.g. by a small oscillating piezo-ceramic membrane.

The flow is excited using a pulsating jet emanating from the flap shoulder near the leading edge. For this specific test model the actuator design is a compromise of cost, performance, size, robustness and flexibility in operation. Fast switching solenoid valves and compressed air are used in order to produce a pulsed wall jet that emanates from a small spanwise oriented slot. Although the valves are small they do not fit inside the hollow flap. In a trade-off between excitation system complexity and actuator performance, all twelve valves are placed inside the fuselage and connected to small chambers (span about 90 mm) in the flap via compressed air lines. As the twelve valves are individually addressable, 2D and 3D excitation modes and spanwise-distributed excitation are possible. Although the necessary tubing has a negative effect on excitation amplitude and frequency due to pressure losses and damping effects, quite a wide range of F^+ and C_μ can be achieved. The valves are very reliable, having never failed even during long run tests. Placing the valves inside the fuselage enables a very easy replacement once more powerful valves are available. The excitation system is calibrated in still air prior to the wind tunnel test using a single hot wire and a 3D-traverse system. However, calibrated C_μ-values can not be given at this time because of a last minute change in the actuator design which is not covered in the original calibration. As the calibration for all frequencies, amplitudes and duty cycles is a long lasting procedure the ratio of the time averaged jet velocity and the free stream velocity is given (calculated from the mass flow values) as an indication for the excitation amplitude. The cited amplitude values are within $\pm20\%$ of the quoted values. Figure 6 displays the actuator assembly.
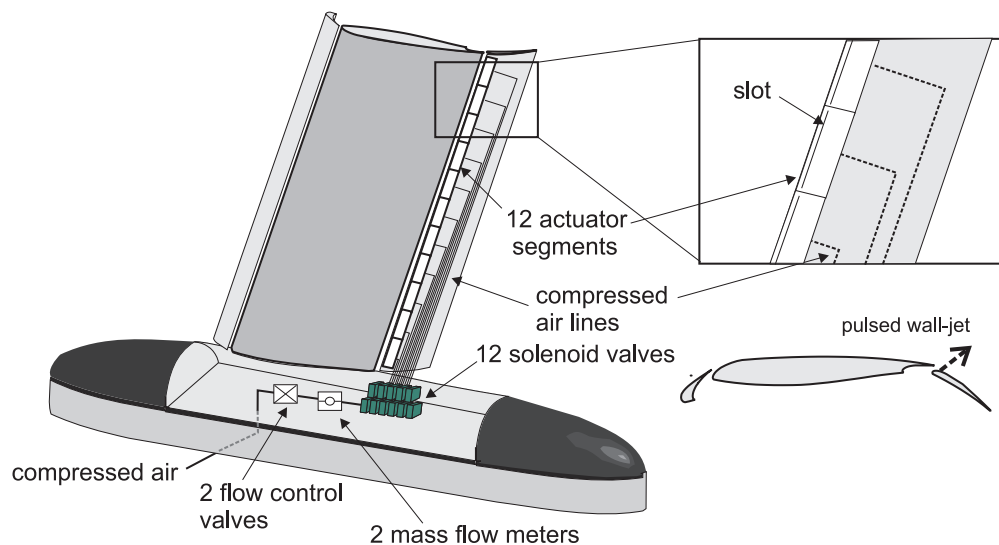

Figure 6. Actuator assembly.

IV.   Unexcited Flow

As this set-up is completely three-dimensional, the investigations of the unexcited flow are aiming at understanding the separation process on the flap and determining the main drivers that trigger flow separation. Factors such as the sweep angle of $30°$ generate a strong cross flow on the main wing and especially on the flap. The finite wing span in the experiment with a low aspect ratio (AR = 2.5), and the flap span equal to the wing span produce a strong wing tip vortex which intensifies the cross flow. Figure 7 gives some impressions of the wall bounded flow on the configuration in the unexcited case. The left hand picture shows tufts on the flap at deflection angle of $\delta_f = 33°$ near the onset of separation. The streamlines on the upper surface of the flap bend towards the wing tip due to local static pressure differences caused by the sweep angle. The surface streamlines in the outer part of the flap proceed almost parallel to the trailing edge of the flap, whereas the streamlines in the inboard flap section are still fully attached. The cross flow gets stronger as the deflection angle approaches its maximum value and flow separation occurs. Once the flow separates, the lift decreases causing the wing tip vortex to lose strength. As a result, no strong cross flow can be observed and the wool tufts show a highly unsteady flow field.
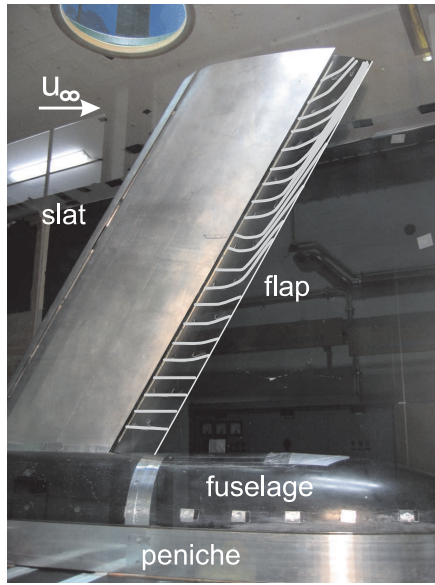
(a) Wool tuft visualization on the flap showing a massive cross flow in the wing tip direction, $Re_c = 0.5 \cdot 10^6, \alpha = 6°, \delta_f = 33°$ (wool tufts are traced for better visibility).
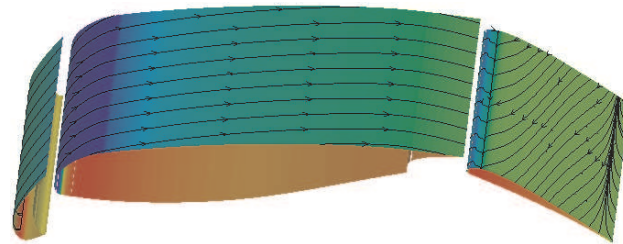
(b) Surface streamlines showing a slight cross flow on the main wing due to the wing sweep and a massive cross flow on the flap. $Re_c = 1 \cdot 10^6, \alpha = 6°, \delta_f = 32°$ (pressure contours)

Figure 7. Qualitative comparison of surface streamlines obtained from experiment and CFD.

The picture on the right hand side of figure 7 displays a corresponding numerical result showing surface streamlines. The cross flow observed in the experiment is clearly seen on the flap as well as on the main wing. Results of all URANS-simulations were generated by fully turbulent flow on all elements. In order to provide separated flow conditions that can be controlled by active methods, different flap settings have been tested. For four different angles of deflection, starting from the baseline configuration ($\delta_f = 32°$), steady computational investigations have been performed. Figure 8 shows the effect of flap deflection on the flow field for $\delta_f = 32°$ and $\delta_f = 37°$. Iso-contours in figures 8(a) and 8(b) give an idea of the expanding separated region with recirculation above the flap by increased flap deflection. As a result of this expanded separation, the detachment position moves from 13% relative chord at $\delta_f = 32°$ to 6% relative chord at $\delta_f = 37°$ (see figures 8(c) and 8(d)). The streamlines on the surface of the main airfoil (7(b)) show the three-dimensional component of the flow produced by the local pressure gradient in the spanwise direction. On the upper surface of the flap, flow separation becomes visible by the direction of surface streamlines (see figures 8(c) and 8(d)). The large recirculation region downstream of the detachment line is based on near-wall flow in the upstream direction with a dominant component in the spanwise direction. This component is also produced by the sweep and is strongly developed in the slow detached flow. The behaviour of the strong cross flow is clearly visible in the large vortices shed from the flap trailing edge, which show a twisted character (figure 14(a)). The larger recirculation region behaves like a flap with less effective camber and produces a lower suction peak. The upwash-effect reduces the velocity near the wall of the main trailing edge. Thereby the flow above the main trailing edge is subject to separation. If the angle of deflection is increased beyond $\delta_f = 37°$, the detachment position remains unchanged.

In the unexcited case the separated flow of the infinite wing is mainly governed by large vortices shedding from the flap trailing edge and interacting with the vortices generated in the shear-layer between the recirculation region and the flow passing through the slot between the main airfoil and flap nose (figure 13(a)). Thereby the unsteady structures are approximately characterised by a two-dimensional behaviour. The spectrum of the lift coefficient of the natural flow shows a dominant amplitude for a Strouhal number formed with the flap chord of $St = F \frac{c_k}{u_\infty} = 0.3$, mainly produced by this vortex-shedding.

As a matter of course, the separation on the flap is also visible in the corresponding lift and drag curves, which are shown in figure 9 for three selected flap deflection angles. At a deflection of $\delta_f = 20$ the flow on the flap is fully attached until the flow separates on the main wing at $\alpha = 28$. Increasing the flap deflection
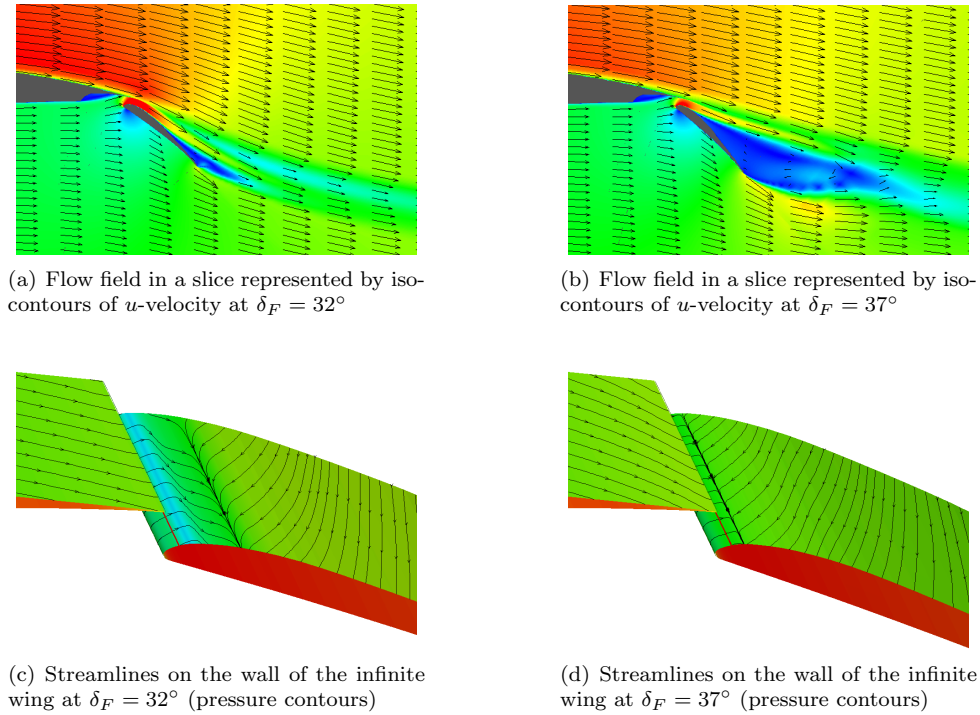
American Institute of Aeronautics and Astronautics

(a) Flow field in a slice represented by iso-contours of u-velocity at $\delta_F = 32°$

(b) Flow field in a slice represented by iso-contours of u-velocity at $\delta_F = 37°$

(c) Streamlines on the wall of the infinite wing at $\delta_F = 32°$ (pressure contours)

(d) Streamlines on the wall of the infinite wing at $\delta_F = 37°$ (pressure contours)

Figure 8. Flow condition on and above the flap with increasing deflection angle

shifts the lift curve to higher c_L values and increases the drag. At high angles of attack (near $c_{L_{max}}$) the lift increase due to the larger flap deflection almost vanishes which is a good indication (in combination with flow visualization) that parts of the flap are partially separated (in this case the outer part separates first). Once the flap angle is set to very high deflections the flow on the flap is fully separated resulting in a lower $\partial c_L/\partial \alpha$ and a lower $c_{L_{max}}$. This setting has also the highest total drag. Due to the measurement with a balance system the total drag can not be split into form drag and induced drag.
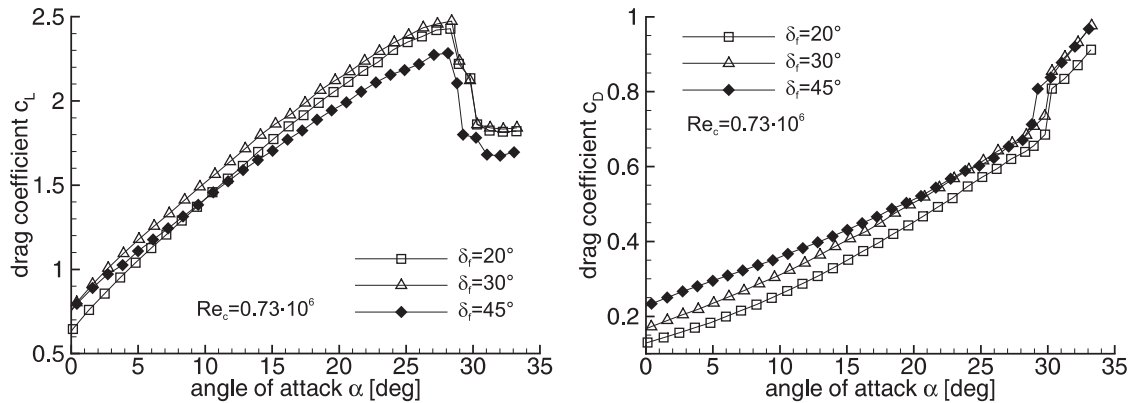

Figure 9. Lift versus angle of attack for different flap deflection angles (unexcited)

V. Excited Flow

V.A. Numerical Simulations

After the base flow investigations, flow control mechanisms are applied. All flow control computations use the baseline case solutions as initial flow conditions. In order to find an optimum excitation, simulations

American Institute of Aeronautics and Astronautics

with different frequencies at $C_\mu = 50 \times 10^{-5}$ as well as with different intensities at $F^+ = 0.6$ are performed. The excitation mode in the 3D simulations of the infinite wing is equal to a sinusoidal blowing and suction. The two-dimensional preliminary investigations employed sinusoidal perturbation and periodic blowing in comparison to the experimental excitation mode.
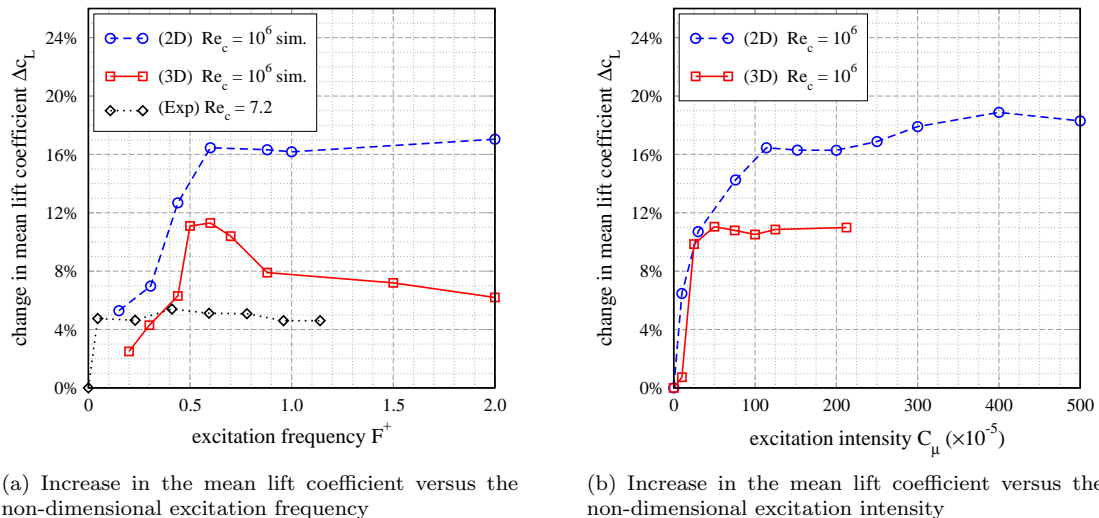

(a) Increase in the mean lift coefficient versus the non-dimensional excitation frequency

(b) Increase in the mean lift coefficient versus the non-dimensional excitation intensity

Figure 10. Numerical results of the excited flow of the infinite wing

Figure 10(a) presents two and three-dimensional results of the excitation in the simulation with different frequencies compared to the three-dimensional results of the measurement. The diagram shows the difference of the lift coefficient relating to the unexcited case depending on excitation frequency. The largest lift of the two-dimensional flow can be found at a frequency of $F^+ = 2.0$, but the largest lift with the lowest drag can be found at $F^+ = 0.6$. In this case the lift coefficient can be enhanced by 17% compared to the baseline simulation. Computations of the infinite swept wing show a similar behaviour with periodic suction and blowing, although the level of gain in lift by the excitation of the two-dimensional case cannot be achieved. The lift coefficient of the infinite swept wing can be enhanced by 11% compared to the baseline simulation at a non-dimensional frequency of $F^+ = 0.6$. The reason for the smaller enhancement for the infinite swept wing compared to the two-dimensional case is the three-dimensionality of the flow induced by the sweep (figure 7). The optimal excitation frequency is slightly larger than the frequency of detaching vortices without excitation ($St = 0.3$). The change in lift of the 3D simulation with excitation is higher in comparison to the experiment, which is ascribed to the effect of the finite wing and with it that of the wing tip vortex. In the range of strong gain in lift ($F^+ = 0.2 \ldots 0.5$) the infinite wing achieved the same change in lift at higher frequencies compared to the two-dimensional flow. At frequencies slightly higher than the optimal excitation frequency the gain in lift is decreased in the case of the infinite wing.

The effect of flow control by periodic blowing of the finite wing is different. The measured results show an almost frequency-independent behaviour of the change in lift. A small optimum is visible at a frequency of $F^+ = 0.4$. Previous experimental investigations[1] of flow control with periodical excitation show the same frequency-dependent behaviour as the present numerical study. So the different behaviour of the excited flow of the finite wing could be a effect of the wing tip vortex. This effect will be investigated in further three-dimensional simulations of the finite wing without the generic fuselage (see III).

Excitation with low intensity ($C_\mu = 10 \ldots 50 \times 10^{-5}$) leads to a strong increase in lift (max. 11%) at the case of the infinite wing (10(b)). If C_μ becomes larger than 50×10^{-5}, however, the lift ceases to increase further. The two-dimensional excited flow shows a similar behaviour (17%), but at intensities greater than $C_\mu = 200 \times 10^{-5}$ the lift becomes slightly increased again (max. 19%). The comparison with the experimental investigations at various momentum coefficients is currently not available, because the calibration of the measured results are still outstanding. In general, the results for both excitation parameters show that the lift either cease to increase or begins to decrease slightly if the frequency or intensity exceeds a certain limit ($F^+ = 0.6$, $C_\mu = 50 \times 10^{-5}$).

Figure 11 shows the gain in lift of each particular element (slat, main wing, flap) of the infinite configuration compared to the baseline simulation at various excitation frequencies. In the right separated area of

the diagram the portions of the total lift coefficient without excitation are represented. However, the largest part of total lift ($\approx 80\%$) are produced by the main wing in the unexcited as well as the excited case. The gain in lift of the perturbed flow is also primarily generated by the main airfoil (max. 8.4% of 11.3 % in total). Through active flow control by means of periodic blowing and suction of the flow over the flap the particular gain in lift of the slat as well as the main airfoil are increased by the *upwash*. Thereby the increase of the slat and main airfoil show a similar effect to the total gain in lift. On the other hand the change in lift of the flap is different. From this behaviour it would appear that the total gain in lift is not caused by the particular increase of the flap but the enhanced circulation around the main airfoil generated by decreased flow separation on the upper flap surface.
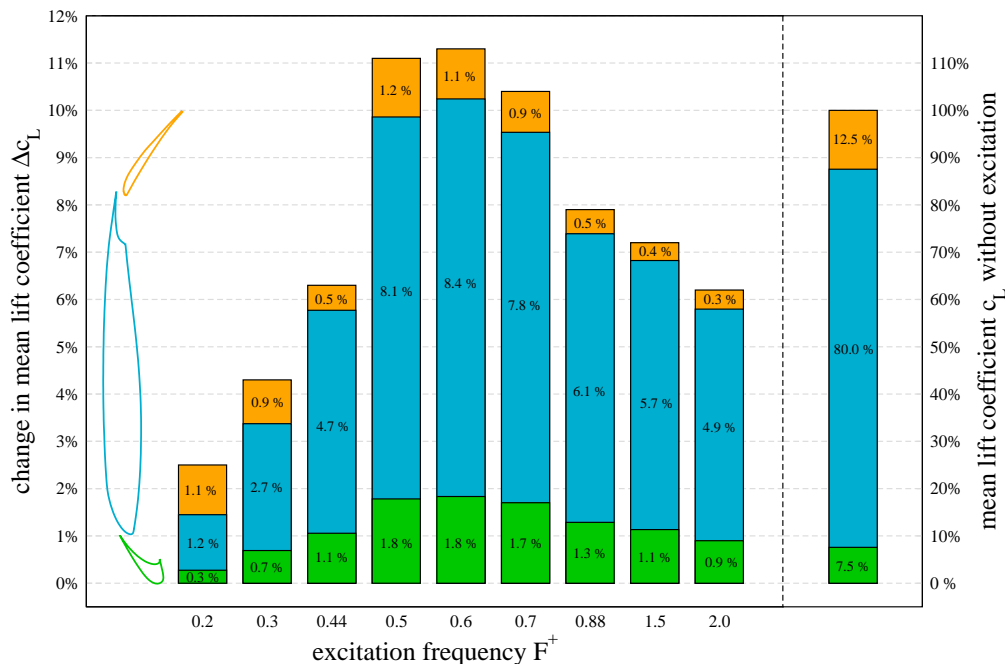

Figure 11. Gain in particular lift at different excitation frequencies

The effect is also identifiable through the behaviour of the blade exit angle behind the trailing edge of the main airfoil (12(c) and 12(d)). Through optimal flow excitation at the flap the blade exit angle of the main airfoil could be extend from 3° (natural flow) to 8° compared with the angle of attack (6°). The reason for the effectiveness of periodic excitation are the vortices generated by the perturbation. Using the method of feature-based comparison of flow fields developed by the Zuse Institute Berlin (ZIB),[24–27] the time-dependent behaviour of the dominant structures and their size in the unforced and forced flow could be identified. The extraction of features as well-defined geometric objects is a prerequisite for distance measurements and extent quantifications. Figures 12(a) and 12(b) show the extracted core lines of the dominant vortices, scaling with the value of the vortex core criterion λ_2 and tinted with the contour-color of the pressure distribution. The natural flow above the flap is mainly governed by large-scale vortex shedding from the flap trailling edge which is nearly eliminated in the optimal excited flow (see figures 12 and 13). Small-sized vortices generated by periodic suction and blowing above the perturbation slit enable the transport of energy from the main flow to the recirculation near the wall. Thereby the time-average detachment position moves downstream, the recirculation area is reduced and the downflow condition is modified. Figure 14 shows this effect. The large swirled vortex above the flap trailling edge in the natural flow dissapears with the excitation, more upstream two small swirled vortices are generated and the strong cross flow near the flap surface is clearly narrowed. The character of the optimum perturbed structures is deeply three-dimensional (see figures 13(b) and 12(c)) whereby the distribution of perturbation energy is improved and the generation of large coherent vortices is suppressed.

All investigations by means of pulsed blowing are carried out by two-dimensional simulations. The studies with variable excitation frequencies and intensities show that active flow control by pulsed blowing could not achieve the gain in lift seen for excitation by periodic suction and blowing. The change in lift is dependent on the duty cycle used (see figure 15(b)). The duty cycle is defined as the blowing duration applied to the cycle
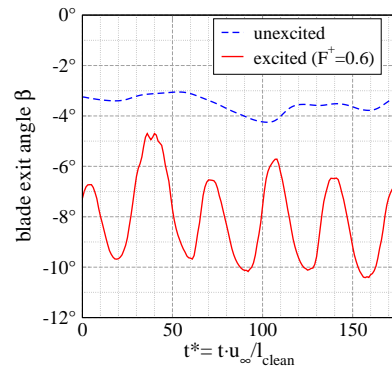
American Institute of Aeronautics and Astronautics
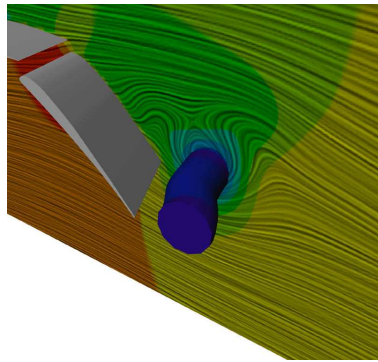
(a) Unexcited
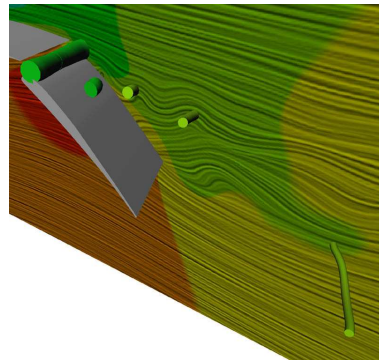
(b) Excited ($F^+ = 0.6, C_\mu = 50 \times 10^{-5}$)
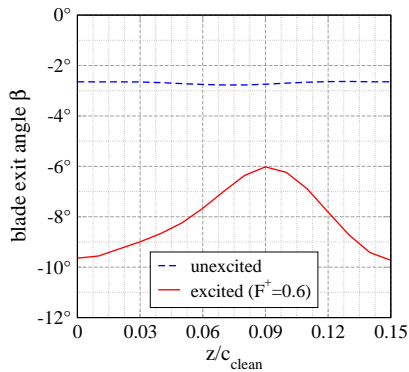

(c) At a point in time

(d) Averaged in spanwise direction

Figure 12. Lines of vortex cores and blade exit angle on the main airfoil trailing edge

duration of the excitation. Only a duty cycle among 20% ($\Delta c_L \approx 10\%$) and 60% ($\Delta c_L \approx 8.5\%$) ensures an obvious gain in lift. Thereby the optimum is found at a duty cycle of 40% ($\Delta c_L \approx 14.5\%$). All investigations by means of pulsed blowing with different excitation frequencies/intensities are carried out by a duty cycle of 50%.
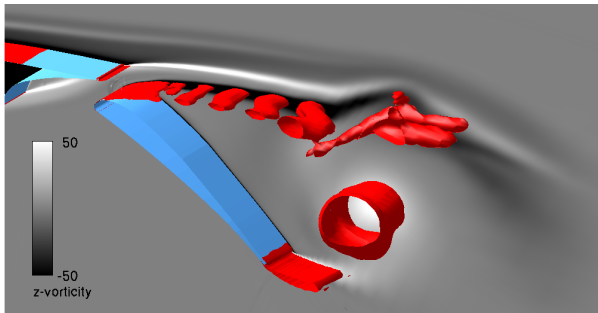
(a) Snapshot of the unexited flow
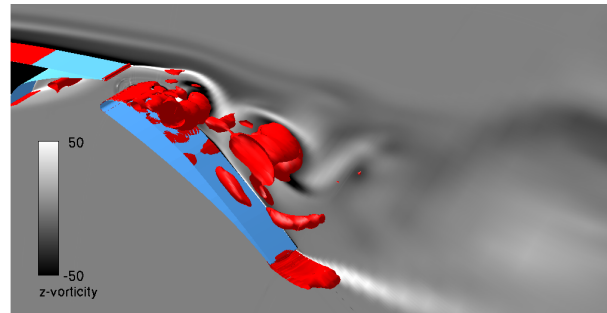
(b) Snapshot of the optimal excited flow

Figure 13. Visualisation of the flow near of the flap (iso-contour of λ_2[red] with contours of z-vorticity [grey])

An another excitation parameter which was investigated by means of periodic suction and blowing is the angle of blow out. At an angle of 90° the flow is perturbed perpendicular to the surface and at a theoretical angle of 180° the flow is perturbed horizontal in upstream direction. Figure 15(a) shows that as the blow-out angle is increased the increase in lift becomes greater until a value of 60° is reached, following which the lift increase remains constant.
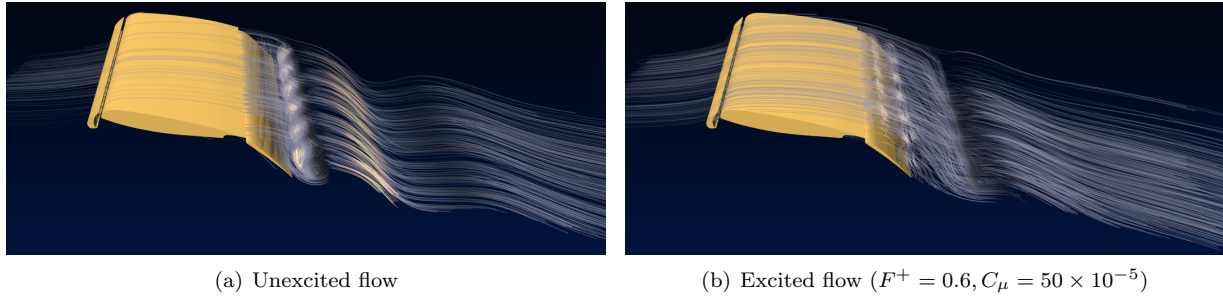
American Institute of Aeronautics and Astronautics

(a) Unexcited flow

(b) Excited flow ($F^+ = 0.6, C_\mu = 50 \times 10^{-5}$)

Figure 14. Illuminated streamlines showing the 3d character of the flow above the flap of the infinite wing

(a) Increase in the mean lift coefficient versus the angle of exit

(b) Increase in the mean lift coefficient versus the duty cycle of pulsed blowing
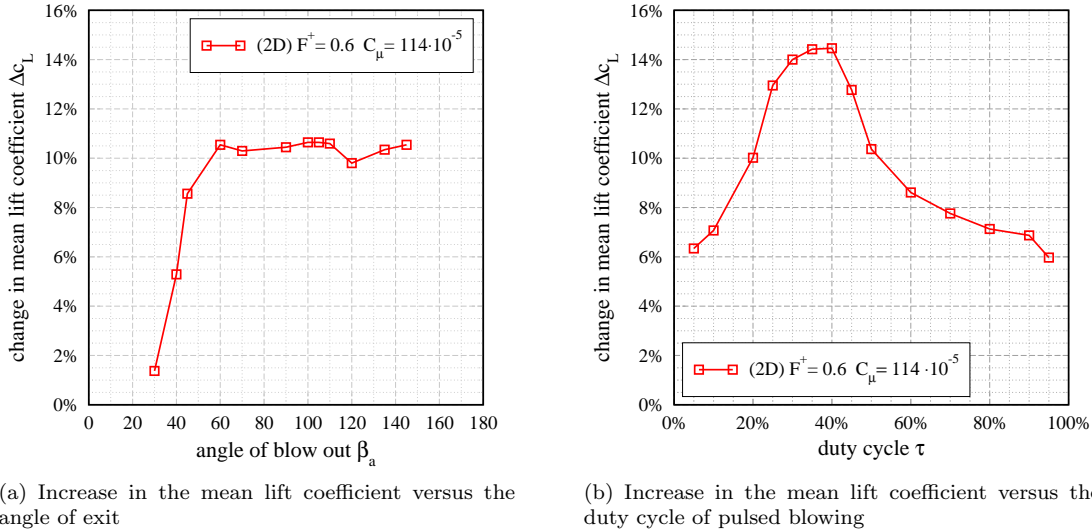
Figure 15. Effect another excitation parameters at the 2D flow field

V.B. Experiments

The experimental results have been conducted at various Reynolds numbers reaching from very low ($Re_c = 0.3 \cdot 10^6$, $u_\infty = 10 m/s$) to a maximum of about $Re_c = 0.85 \cdot 10^6$ ($u_\infty = 29 m/s$). Most of the results presented in this manuscript were gathered at a Reynolds number of around $0.7 \cdot 10^6$ ($u_\infty = 25 m/s$) which is close to the Reynolds number used in the numerical investigation. Besides investigations of excitation frequency, amplitude, duty cycle and various different excitation modes covered in the numerical part, the main interest in the experiment is the influence of periodic forcing on the aerodynamic forces (primarily lift and drag) for different high-lift settings and Reynolds numbers. Figure 16 displays exemplary lift curves with and without forcing. The angle of attack is fixed at $\alpha = 6°$ while only the flap deflection is increased in one degree steps from $\delta_f = 14°$ to $\delta_f = 45°$. The base flow lift curve (line with square symbols, left hand side diagram) shows a constant or slightly decreasing lift once the flap deflection is higher than $\delta_f = 30°$. At higher angles above $\delta_f = 40°$ the lift drops clearly indicating a separated flow on the flap. Once active flow control is turned on, separation is prevented shifting the curve to the left and to higher lift values. The increase in lift even at very low flap deflection is due to the separated flow behind the flap tracks (covered by fairings) that is suppressed by active flow control. But even at higher deflection angle where the flow starts to separate from the complete flap, unsteady forcing is able to keep the flow attached resulting in an increased lift compared to the base flow without forcing. There are a lot of parameters influencing the result that depend on the initial condition of slot location and wall jet direction. As compressed air and valves are used to exite the flow, unsteady excitation is easily compared to steady blowing by opening the valves. The right hand side diagram shows a selected result taken at a low Reynolds number of $Re_c = 0.34 \cdot 10^6$ because at higher Reynolds numbers the ratio of mean jet velocity and free stream velocity decreases. One reason is the necessary tube length between valve and slot location that causes severe pressure losses. For a specific

high-lift setting the data shows very clearly that unsteady forcing is more effective than steady blowing in this case especially at very low jet velocities. Figure 17 display the benefit of unsteady forcing during an
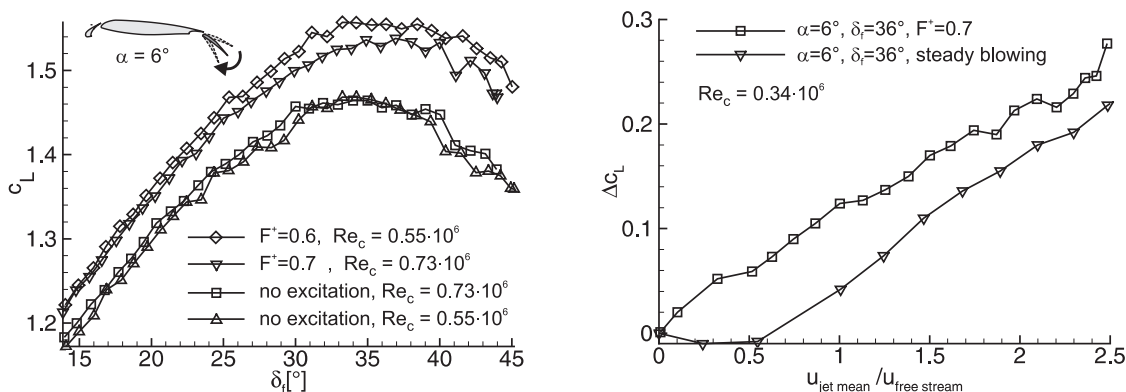

Figure 16. Lift versus flap deflection angle with and without periodic forcing

angle of attack sweep. The flap is set to $\delta_f = 35°$ resulting in an almost complete separation on the flap. Forcing the flow throughout the complete α-range reattaches the flow and keeps it attached until maximum lift is reached and the flow separates from the main element. Because the configuration investigated has a finite wing span the shown drag curves behaves differently. Although the separation on the flap is suppressed the base flow drag and the excited flow drag show almost identical values at low angles of attack. This is due to the fact that form drag is decreased but at the same time the higher lift case by the now attached flow increases the lift depended induced drag. At higher angles of attack and especially near the maximum lift the total drag in the excited case is even slightly higher the base flow drag. Once the flow separates in both cases on the main wing the drag curves again show identical values. Although unsteady forcing prevents separation and is able to increase lift, the higher induced drag increases the drag as well. Looking at the lift-to-drag ratio plotted in the right hand side of figure 17 clarifies this behaviour. Improvements in the lift-to-drag ratio can only be achieve in the low α-domain.
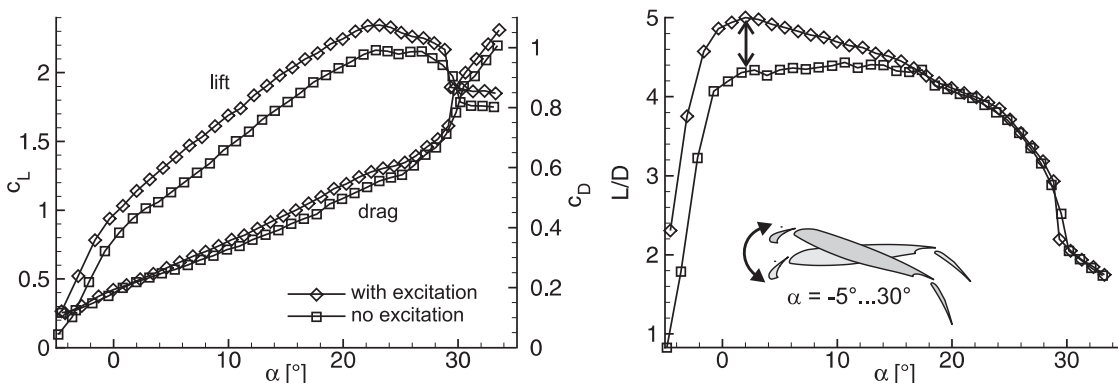

Figure 17. Lift and drag against angle of attack with and without flow control ($\delta_f = 35°$, $Re_c = 0.52 \cdot 10^6$)

VI.   Conclusion

Active flow control by means of periodic suction and blowing as well as pulsed blowing into the flap boundary layer has been applied to a three-element high lift configuration. Experimental and numerical investigations have shown that the flow field can be successfully controlled. Leading edge separation on the flap can be delayed and the lift can significantly be enhanced. The numerical part mainly focussed on the mechanisms of separation control by analysing flow field structures at different excitation parameters, whereas the main emphasis of the experimental investigation lay on the overall lift and drag improvement by measuring integral values. The experiment was conducted using a half-model with finite span, wing sweep and fuselage whereas the numerical investigation was carried out on a swept wing of infinite span.

American Institute of Aeronautics and Astronautics

For the experiments without excitation, the influence of the flap deflection on the flow over the flap and with it the behaviour of the overall lift and drag coefficient was studied. At larger flap deflection the lift and the drag were increased. If the flap angle was set very high deflections ($\delta_f = 45°$), the maximum lift coefficient c_{Lmax} was diminished and $\partial c_L/\partial \alpha$ became smaller. The drag increased continously.

In order to provide separated flow conditions in the numerical part various flap settings have been tested. At a deflection angle of $\delta_f = 37°$ ($\alpha = 6°$) the flow on the flap is fully detached.

The sweep generated a strong cross flow on all parts of the configuration especially on the seperated flap flow. The wing tip vortex of the finite wing was thereby strengthened and the vortex shed from the flap trailing edge showed a twisted character.

Active flow control by means of oscillatory suction and blowing was found to be much more efficient with respect to lift than pulsed blowing. On the other hand the data of the experiments show that unsteady blowing is more effective than steady blowing at a specific high-lift setting. In general, active flow control is able to reattach the flow resulting in an inereased lift compared to the base flow for various angles of attack and flap deflections.

By changing the excitation frequency at a constant intensity, an optimum frequency can be identified. The measured results of the finite wing showed an almost frequency-independent behaviour of gain in lift. The mean lift coefficient of the two-dimensional flow increases by 17%, of the infinite wing by 11% and in the measurement of the finite wing by 6%. The significant differences between the gains in lift is explained by the growing three-dimensional effect.

Numerical investigations with various momentum coefficients at a given excitation frequency have shown that the lift increases strongly if the intensity is smaller than $C_\mu = 50 \times 10^{-5}$. If C_μ becomes larger, however, the lift ceases to increase further (infinite wing) or increases again slightly (2D flow).

The largest part of total lift ($\approx 80\%$) are produced by the main wing in the unexcited as well as the excited case. The study of the gain in lift of each particular element of the infinite configuration showed that the total gain in lift is not caused by the particular increase of the flap but the enhanced circulation around the main airfoil generated by decreased flow separation on the upper flap surface. The reason for the effectiveness of periodic excitation are the vortices generated by the perturbation. As the natural flow above the flap is mainly governed by large-scale vortex shedding from the flap trailing edge, three-dimensional, small-scale vortices generated by periodic suction and blowing above the perturbation slit enable the transport of energy from the main flow to the recirculation near the wall.

Other excitation parameters such as the duty cycle of pulsed blowing and the angle of blow out were investigated by means of two-dimensional simulations. A optimum was found at a duty cycle of 40% ($\Delta c_L \approx 14.5\%$) and at an angle of blow out larger than 60° ($\Delta c_L \approx 11\%$).

Acknowledgments

References

[1]F.H. Tinapp. *Aktive Kontrolle der Strömungsablösung an einer Hochauftriebs-Konfiguration*. PhD thesis, Technische Universität Berlin, 2001.

[2]M. Schatz and F. Thiele. Numerical study of high-lift flow with separation control by periodic excitation. *AIAA Paper 2001-0296*, 2001.

[3]M. Schatz, F. Thiele, R. Petz, and W. Nitsche. Separation control by periodic excitation and its application to a high lift configuration. *AIAA Paper 2004-2507*, 2004.

[4]A.A. Hassan and R.D. Janakiram. Effects of zero-mass synthetic jets on the aerodynamics of the NACA-0012 airfoil. *AIAA Paper 97-2326*, 1997.

[5]D. Greenblatt and B. Nishri. Dynamic stall control by periodic excitation, part 2: Mechanisms. *Journal of Aircraft*, 38(3), 2001.

[6]D. Postl, A. Gross, and H.F. Fasel. Numerical investigation of active flow control for low-pressure turbine blade separation. *AIAA Paper 2004-0750*, 2004.

[7]J. Rullan, P.P. Vlachos, D.P. Telionis, and M.D. Zeiger. Flow control of sharp-edged wings via unsteady blowing. *AIAA Paper 2004-0226*, 2004.

[8]D.V. Maddalon, F.S. Collier, L.C. Montoya, and C.K. Land. Transition flight experiments on a swept wing with suction. *AIAA Paper 89-1893*, 1989.

[9]A. Seifert, A. Darabi, and I. Wygnanski. On the delay of airfoil stall by periodic excitation. *Journal of Aircraft*, 33(4), 1996.

[10]F. Tinapp and W. Nitsche. On active control of high-lift flow. In W. Rodi and D. Laurence, editors, *Proc. 4th Int. Symposium on Engineering Turbulence Modelling and Measurements, Corsica*. Elsevier Science, 1999.

[11]E.G. Paterson and W.J. Baker. Simulation of steady circulation control for marine-vehicle control surfaces. *AIAA Paper 2004-0748*, 2004.

[12]S.S. Ravindran. Active control of flow separation over an airfoil. TM-1999-209838, NASA, Langley, 1999.

[13]L.D. Kral, J.F. Donovan, A.B. Cain, and A.W. Cary. Numerical simulation of synthetic jet actuators. *AIAA Paper 97-1824*, 1997.

[14]J.F. Donovan, L.D. Kral, and A.W. Cary. Active flow control applied to an airfoil. *AIAA Paper 98-0210*, 1998.

[15]I. Wygnanski. The variables affecting the control separation by periodic excitation. *AIAA Paper 2004-2505*, 2004.

[16]M. Gad-el Hak. Flow control: The future. *Journal of Aircraft*, 38(3), 2001.

[17]L. Pack Melton, C.-S. Yao, and A. Seifert. Active control of separation from the flap of a supercritical airfoil. *AIAA Journal*, Vol. 44(No. 1):pp. 34–41, 2006.

[18]A. Seifert, A. Darabi, and I. Wygnanski. Delay of airfoil stall by periodic excitation. *Journal of Aircraft*, Vol. 33(No. 4):pp. 691–698, July-August 1996.

[19]R. Meyer and D.W. Bechert. Beeinflussung von Strömungsablösungen an Tragflügeln. Abschlussbericht, Hermann-Föttinger-Institut, TU Berlin, 1998.

[20]L. Koop. *Aktive und Passive Strömungsbeeinflussung zur Reduzierung der Schallabstrahlung an Hinterkanntenklappen von Tragflügeln*. PhD thesis, Technische Universität Berlin, 2005.

[21]K. Kaepernick, L. Koop, and K. Ehrenfried. Investigation of the unsteady flow field inside a leading edge slat cove. In *11th AIAA/CEAS Aeroacoustics Conference (26th Aeroacoustics Conference), Monterey, CA, USA*, 2005.

[22]T. Rung and F. Thiele. Computational modelling of complex boundary-layer flows. In *9th Int. Symp. on Transport Phenomena in Thermal-Fluid Engineering, Singapore*, 1996.

[23]M. Schatz. *Numerische Simulation der Beeinflussung instationärer Strömungsablösung durch frei bewegliche Rückstromklappen auf Tragflügeln*. PhD thesis, Berlin University of Technology, Mensch & Buch Verlag, Berlin, 2003.

[24]H. Theisel, T. Weinkauf, H.-C. Hege, and H.-P. Seidel. Topological methods for 2D time-dependent vector fields based on stream lines and path lines. *IEEE Transactions on Visualization and Computer Graphics*, 11(4):pp. 383–394, 2005.

[25]K. Shi, H. Theisel, T. Weinkauf, H. Hauser, H.-C. Hege, and H.-P. Seidel. Path line oriented topology for periodic 2D time-dependent vector fields. In *Proc. Eurographics / IEEE VGTC Symposium on Visualization (EuroVis '06)*, pages pp. 139–146.

[26]H. Theisel, J. Sahner, T. Weinkauf, H.-C. Hege, and H.-P. Seidel. Extraction of parallel vector surfaces in 3D time-dependent fields and application to vortex core line tracking. In *Proc. IEEE Visualization 2005*, pages pp. 631–638.

[27]J. Sahner, T. Weinkauf, and H.-C. Hege. Galilean invariant extraction and iconic representation of vortex core lines. In *Proc. EuroVis 2005*.